LARGE HIGHLY IONIZED NEBULAE AROUND ULTRA-LUMINOUS X-RAY SOURCES

Dae-Sik Moon[1], Fiona A. Harrison[2], S. Bradley Cenko[3], and Jamil A. Shariff[1]
[1] Department of Astronomy and Astrophysics, University of Toronto, Toronto, ON M5S 3H4, Canada; moon@astro.utoronto.ca, shariff@astro.utoronto.ca
[2] Space Radiation Laboratory, California Institute of Technology, MS 320-47, Pasadena, CA 91125, USA; fiona@srl.caltech.edu
[3] Department of Astronomy, University of California, Berkeley, CA 94720-3411, USA; cenko@astro.berkeley.edu
Received 2011 January 3; accepted 2011 March 11; published 2011 March 29

ABSTRACT

We present the results of deep optical spectroscopic observations using the LRIS spectrograph on the Keck I 10 m telescope of three ultra-luminous X-ray sources (ULXs): Ho IX X-1, M81 X-6, and Ho II X-1. Our observations reveal the existence of large (100–200 pc diameter) highly ionized nebulae, identified by diffuse He II λ4686 emission, surrounding these sources. Our results are the first to find highly ionized nebulae of this extent, and the detection in all three objects indicates this may be a common feature of ULXs. In addition to the extended emission, Ho IX X-1 has an unresolved central component containing about one-third of the total He II flux, with a significant velocity dispersion of $\simeq$370 km s^{-1}, suggestive of the existence of a photoionized accretion disk or an extremely hot early-type stellar counterpart. Most of the He II emission appears to be surrounded by significantly more extended Hβ emission, and the intensity ratios between the two lines, which range from 0.12 to 0.33, indicate that photoionization is the origin of the He II emission. Sustaining these extended nebulae requires substantial X-ray emission, in the range $\sim$10^{39}–10^{40} erg s^{-1}, comparable to the measured X-ray luminosities of the sources. This favors models where the X-ray emission is isotropic, rather than beamed, which includes the interpretation that ULXs harbor intermediate-mass black holes.

Key words: black hole physics – galaxies: individual (Holmberg IX, M81, Holmberg II) – ISM: bubbles – ISM: kinematics and dynamics – X-rays: galaxies

1. INTRODUCTION

Ultra-luminous X-ray sources (ULXs) are bright point-like sources found at off-nuclear positions in nearby galaxies. If the X-ray emission is isotropic, the ULX luminosities would be in the range 10^{39}–10^{41} erg s^{-1}, with corresponding Eddington-limited masses in excess of 100 $M_\odot$. This leads to the suggestion that ULXs are black holes with mass intermediate between stellar-mass systems and very massive nuclear black holes of galaxies. The large luminosities, however, may still originate from stellar-mass black holes if the X-ray emission is beamed, or if accretion disks are capable of radiating at super-Eddington rates (e.g., King et al. 2001; Begelman 2002). Indeed, some X-ray binaries are known to produce super-Eddington luminosities, reaching $\gtrsim$10^{41} erg s^{-1} in their flaring states (e.g., Moon & Eikenberry 2001; Moon et al. 2003a, 2003b; Sivakoff et al. 2005). The nature of ULXs is still quite uncertain, and given they are broadly selected as bright off-nuclear X-ray sources, they may represent a mixture of different types of objects (Zampieri & Roberts 2009).

Many ULXs have early-type stars as optical counterparts, indicating their binary nature. Some also have extended optical nebulae surrounding the central source (see Pakull & Mirioni 2002, for early results). Of particular interest is the detection of the He II line at 4686 Å (He II λ4686) in the immediate vicinity ($\lesssim$2″) of some of bright sources (e.g., Grise et al. 2006; Pakull & Mirioni 2002; Kaaret et al. 2004; Lehmann et al. 2005; Kaaret & Corbel 2009). Because of the very high ionization potential of 54.4 eV, this line emission traces high-energy (EUV to X-ray) radiation fields or extremely strong shocks and is usually considered to be a signpost of X-ray photoionized nebulae (e.g., Pakull & Angebault 1986; Pakull & Motch 1989). Where present, the observed He II λ4686 luminosities have been used to obtain lower limits to the total X-ray ray luminosity (e.g., Kaaret & Corbel 2009), which

provides a constraint central to determining the nature of ULXs.

In this Letter, we present deep spectroscopic observations of the He II λ4686 line in three ULXs: Ho IX X-1, M81 X-6, and Ho II X-1. Ho IX X-1 (= M81 X-9) is located in the dwarf galaxy Holmberg IX near M81 and is known to have variable X-ray emission with a luminosity (assuming isotropic emission) of $\sim$10^{40} erg s^{-1} (La Parola et al. 2001), along with a large ($\geqslant$250 pc in diameter) optical nebula seen in H recombination and forbidden lines (Miller 1995; Grise et al. 2006). Its optical counterpart, which is probably an early-type star of $V \simeq$ 22.8 (Grise et al. 2006), shows strong, broad, spatially unresolved He II λ4686 line emission (Grise et al. 2006); however, Ramsey et al. (2006) were unable to detect extended He II λ4686 emission. M81 X-6 (= NGC 3031 X-11) resides in the spiral galaxy M81 and also shows long-timescale variable X-ray emission with an isotropic-equivalent luminosity of $\sim$2 $\times$ 10^{39} erg s^{-1}. Its optical counterpart is an O8 V star of $V \simeq$ 23.9 situated in a spiral arm with high local stellar density (Roberts & Warwick 2000; Liu et al. 2002) and embedded in an Hα nebula $\sim$150 pc in diameter (Ramsey et al. 2006). Prior to the observations reported here no He II λ4686 emission has been detected in M81 X-6. Ho II X-1 is one of the most luminous ($>$10^{40} erg s^{-1}) ULXs and is located in the dwarf star-forming galaxy Holmberg II. Kaaret et al. (2004) identified a likely optical counterpart that is an early-type star surrounded by a nearby optical nebula including He II λ4686 emission $\sim$2″ in size. Lehmann et al. (2005) confirmed the extended He II λ4686 region of 21 $\times$ 47 pc and determined $B \simeq$ 20.05 mag of the optical counterpart. In addition, this ULX appears to have a radio counterpart (Miller et al. 2005). The observed He II λ4686 luminosity of 2.7 $\times$ 10^{36} erg s^{-1} corresponds to a lower limit on the X-ray luminosity of (4–6) $\times$ 10^{39} erg s^{-1}, assuming that X-ray photoionization is the source of the line excitation (Kaaret et al. 2004).
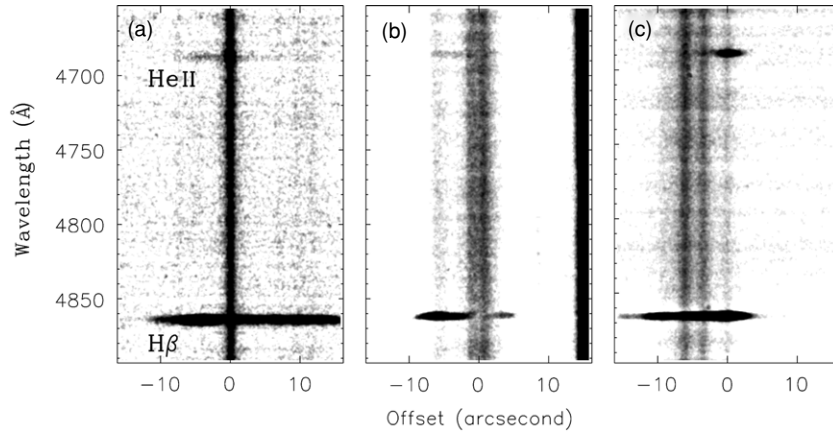
Figure 1. Integrated Keck LRIS spectrograms of the three ULXs—Ho IX X-1 (a), M81 X-6 (b), and Ho II X-1 (c)—in the wavelength range of He II (λ4686) and Hβ (λ4861) lines. The *x*-axis represents the angular distance (in the arcsecond unit) from the optical counterparts of the ULXs. Left is south for (a), west–southwest for (b), and west–northwest for (c).

Table 1
Observing Parameters

Object	Coordinate (J2000)	Position Angle	Date	Exposure
Ho IX X-1	(09:57:53.3, +69:03:48)	0	2007 Mar 24–26	1800 s × 11
M81 X-6	(09:55:33.0, +69:01:13)	72.5	2006 Jan 31, Feb 2–3	1800 s × 9
M81 X-6	(09:55:33.0, +69:01:13)	0	2007 Mar 24–25	1800 s × 5
Ho II X-1	(08:19:29.0, +70:42:19)	108.4	2007 Mar 26	600 s × 2

2. OBSERVATIONS AND RESULTS

The observations of the three ULXs, Ho IX X-1; M81 X-6; and Ho II X-1, occurred 2006 January 31, 2006 February 2–3, and 2007 March 3–5 using the Low Resolution Imaging Spectrograph (LRIS; Oke et al. 1995) on the Keck I 10 m telescope. The *B*-band seeing was 1″5–2″ (2006) and 1″0–1″5 (2007); the slit width and length were 1″ and 120″, respectively. A beam dichroic inside LRIS splits incoming light to the blue and red sides followed by a 600/4000 grism (3010–5600 Å) and a 600/7500 grating (5700–8200 Å). Photometric calibrations were performed with standard sources HD 93521 and HD 9, and wavelength solutions were obtained using arc lamp lines.

Table 1 summarizes the observations. We accumulated multiple exposures of 1800 s each for Ho IX X-1 and M81 X-6, totaling on-source integration time up to 5.5 (Ho IX X-1) and 7.0 (M81 X-6) hr. For Ho II X-1, which is much brighter, we integrated for a total of ~0.3 hr. The slit position angles for Ho IX X-1 and Ho II X-1 were 0° and 108.°4, respectively, while two different position angles, 0° and 72.°5, were used for M81 X-6. We detected extended He II emission surrounding all three objects. The line was not detected in the 0° position angle observations of M81 X-6; however, the signal to noise of these observations makes non-detection consistent with the level seen in the 2006 data. We therefore present the analyses of the 2006 data of M81 X-6 alone. We also detected several Balmer series H lines and forbidden transitions of [O I], [O II], [O III], [Ne III], [N II], and [S II]. Detailed analyses of the entire spectra will be published elsewhere; in this Letter, we concentrate on the He II λ4686 and Hβ line spatial and spectral analysis.

Figure 1 shows integrated spectrograms of the three ULXs in the wavelength range 4650–4900 Å, containing the He II (λ4686) and Hβ (λ4861) lines. The offset (*x*-axis) is in arcseconds relative to the reported position of the optical counterpart in each system. The dispersed continuum emission from the optical counterparts of Ho IX X-1 and Ho II X-1 is clearly visible in Figures 1(a) and (c), respectively. In the Ho II X-1 spectrogram, in addition to the optical counterpart, there are two bright background stars between −3″ and −7″. The counterpart detection in M81 X-6 in Figure 1(b) is uncertain. The dispersed light of its optical counterpart, which is fainter relative to the other two ULXs, appears to be blended with that of many other nearby stars (see Liu et al. 2002). The ≃2″ seeing of these observations makes the continuum from the counterpart impossible to isolate from that of nearby stars. (The bright continuum source at ~15″ to the right in Figure 1(b) is a field star used for the slit alignment.) In all three spectrograms extended He II and Hβ emission is clearly detected.

Figure 2 compares the spatial distribution of the integrated He II and Hβ line intensities (solid line for He II; dotted line for Hβ) along the slit direction, with the same *x*-axis origin used in Figure 1. The Hβ distribution is shifted by an arbitrary constant (0.3) in the *y*-direction for clarity. We subtracted the background, including the stellar continuum, using the flux detected in nearby pixels. A common feature of all three (especially Ho IX X-1 and Ho II X-1) profiles is that, with the exception of the narrow central component in Ho IX X-1, the Hβ spatial profile generally tracks, but is more extended than the He II emission. For all the three ULXs, the He II emission extends to >100 pc from the center, while the Hβ emission extends much further, to beyond 250 pc. The He II λ4686 to Hβ line intensity ratios are ~0.12 (Ho IX X-1), 0.19 (M81 X-6), and 0.33 (Ho II X-1). Below we discuss the spatial distribution for each source.

The He II line intensity distribution in Ho IX X-1 (Figure 2(a)) can be fit using three Gaussian components; the fit is shown as a dashed line. The central, narrow, unresolved component is described by a Gaussian profile with an FWHM of 1″0 (or 17.5 pc), comparable to the seeing size. Its integrated intensity contains ~1/3 of the total He II emission. This component is surrounded by asymmetric emission extending more than
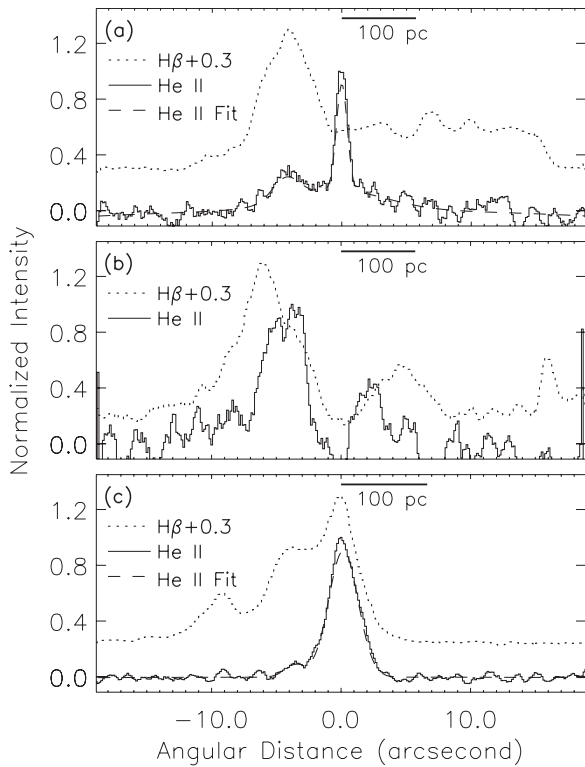
Figure 2. (a) Relative spatial distributions of the integrated He II and Hβ line intensities along the slit directions of Ho IX X-1 Figure 1 (solid line for the He II line intensity distribution; dotted line for the Hβ line), along with the results of Gaussian fittings (dashed line) of the He II line intensity distribution. The solid bar at the top of the plot represents angular distance corresponding to 100 pc. (b) Same as (a), but for M81 X-6 without Gaussian fitting results. (c) Same as (a), but for Ho II X-1.

100 pc in both directions, but more prominently to the south (left). The extended He II emission can be fit using two Gaussian components: one centered at the origin with an FWHM of 8″.7 ($\simeq$150 pc) and the other at $-4″.3$ ($\simeq$ 75 pc) with an FWHM of 2″.4 ($\simeq$ 40 pc). The first component is roughly three times brighter than the second one, and the intensity of the total emission in the south is greater than that in the north by $\sim$40%. We estimate the extent of the He II emission to be 184 ± 20 pc, determined by measuring the continuous area across the center where the signal intensity of each data point is greater than noise level at the 90% confidence level. We estimated the noise level at $< -15″$ and $> +15″$, where there is no apparent He II emission. The Hβ emission of this source is asymmetric without any apparent central peak. With the notable exception of the central peak, however, the Hβ profile is similar in shape to that of the He II. The Hβ spreads somewhat flatly to $\sim$300 pc in the northern direction, whereas, in the south, it extends less ($\sim$200 pc) and peaks where the He II emission has a local peak. The total extension of the Hβ emission, therefore, is $\sim$500 pc, and it is slightly ($\sim$10%) brighter in the south than the north. We estimate the total luminosity of the He II line emission integrated along the slit to be $\sim$3.7 $\times$ 10^{35} erg s^{-1} for a distance of 3.6 Mpc.

There is no identifiable central component to the He II emission in M81 X-6 (Figure 2(b)). The distribution is irregular and not well described by Gaussian components. The He II is extended 115 ± 13 pc west–southwest (left) from the center, whereas it extends 42 ± 7 pc in the opposite direction, for a total width of 167 ± 15 pc. Both the He II and Hβ emission is heavily (>90%) concentrated in the west–southwest where

the Hβ emission extends more than 150 pc. The He II and Hβ emission is again spatially correlated; however, the peak locations of the He II emission appear to be shifted toward the center compared to Hβ. The main peak of the He II emission may be dividable into two components at $x \simeq 4″.5$, although the low signal-to-noise ratio makes it difficult to confirm this. The total measured He II luminosity is $\sim$8.8 $\times$ 10^{34} erg s^{-1} for a distance of 3.6 Mpc.

For Ho II X-1 (Figure 2(c)), the He II emission is well described by a broad, central Gaussian component of 2″.7 ($\simeq$40 pc) FWHM, along with a minor component of 1″.9 ($\simeq$30 pc) FWHM located at $-3″.5$ ($\simeq$ 50 pc) to the west–northwest. The integrated intensity of the former is roughly 10 times greater than that of the latter. The Hβ emission is distributed very similarly to the He II emission: the main peak is at the center and there is a secondary peak near the location of the secondary component of the He II emission at $-3″.5$. In addition, there is a third peak centered at $-10″$ in the Hβ emission. The He II emission is somewhat enhanced at this location, although it is almost indistinguishable from the noise. The size of the He II emission is 122 ± 7 pc. The measured He II luminosity is $\sim$3.6 $\times$ 10^{36} erg s^{-1}, which is slightly greater than that of previous measurements (Pakull & Mirioni 2002; Kaaret et al. 2004; Lehmann et al. 2005), for a distance of 3.1 Mpc.

Figure 3 shows spectral line profiles of the He II (a–c) and Hβ (d–f) transitions for the three ULXs. There are two He II line profiles for Ho IX X-1 and Ho II X-1: the thick solid profiles are for the central emission obtained within 1″ from the center (i.e., the optical counterparts); the thin solid ones are for the extended emission outside the center. The FWHM of the He II lines of the spatially extended emission are 5.0 (Ho IX X-1), 3.7 (M81 X-6), and 3.5 (Ho II X-1) Å. Those for the central emission are 6.7 Å (Ho IX X-1) and 3.6 Å (Ho II X-1). For the Hβ lines, the line widths of the extended emission are 4.4 Å (Ho IX X-1), 3.6 Å (M81 X-6), and 3.5 Å (Ho II X-1). The LRIS instrumental line widths, estimated from the measured widths of the calibration lamp lines, are in the range 3.8–4.1 Å. We therefore conclude that the He II emission of Ho IX X-1, especially the central component, has a contribution from dynamical motion in the source, whereas we can only determine an upper limit of $\sim$250 km s^{-1} for the velocity dispersion of the other lines. For Ho IX X-1, the extra widths correspond to velocity dispersions of 370 km s^{-1} and 230 km s^{-1} for the central and extended components, respectively. These dispersions of the He II lines are consistent with previous observations (Grise et al. 2006) and are larger than those reported in [O III] λ5007 and [S II] λ6717 lines (Abolmasov & Moiseev 2008). For Ho II X-1, the upper limit is consistent with the results of previous observations (Lehmann et al. 2005).

3. DISCUSSION AND CONCLUSIONS

Our deep Keck observations spectroscopically identified spatially extended, highly-ionized He II emission around three ULXs. In the case of Ho IX X-1 and M81 X-6 this is the first reported detection of diffuse He II emission from these systems, and in the case of Ho II X-1 we find the highly ionized region to be larger than previously reported. The sizes we find are in the range of 100–200 pc (in diameter), larger than any previously known He II emission around a compact source. The He II nebulae around extremely hot stellar sources, such as planetary nebulae or stellar X-ray sources, are generally smaller than 10 pc. Previous optical observations of some ULXs, including Ho IX X-1 and Ho II X-1 observed in this study,
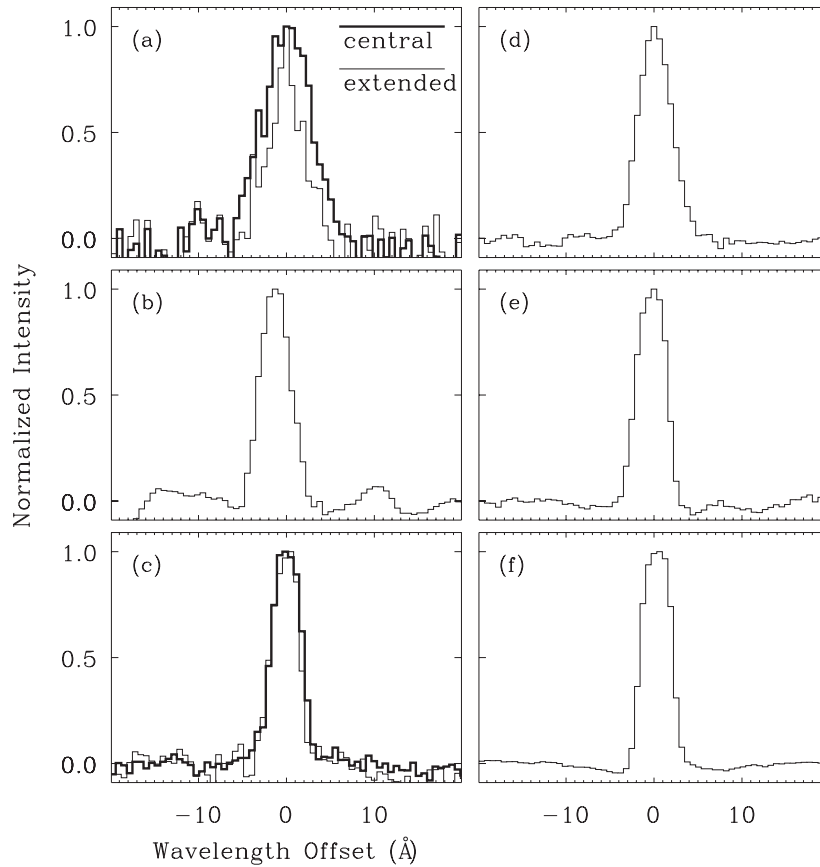
Figure 3. (a) He II λ4686 line profiles for the central (thick solid line) and extended emission (thin solid line) of Ho IX X-1. (b) Same as (a), but for the extended emission of M81 X-6. (c) Same as (a), but for Ho II X-1. (d) Hβ line profile of Ho IX X-1. (e) Same as (d), but for M81 X-6. (f) Same as (d), but for Ho II X-1.

detected He II emission only from the locations of the optical counterparts (e.g., M101 X-1, NGC 1313 X-2, and Ho IX X-1; Kuntz et al. 2005; Pakull et al. 2005; Grise et al. 2006) or from their close (<50 pc) vicinities (e.g., Ho II X-1 and NGC 5408 X-1; Grise et al. 2006; Kaaret & Corbel 2009).

The identification of large He II emission regions surrounding all three sources included in this study indicates that extended, highly ionized nebulae are a common or even ubiquitous feature of ULXs. Previous non-detections likely result from the limited depth of the observations, with Keck LRIS being significantly more sensitive than other telescopes for this purpose. In all three cases, the extended emission contains the majority of the total He II flux. In the case of Ho IX X-1, the central unresolved component amounts to only 1/3 of the total emission, and there is no apparent central component at all in M81 X-6. In Ho II X-1 the He II emission is distributed in a relatively broad (~40 pc FWHM), but very regularly distributed component with a minor contribution from very extended emission in the west–northwest.

A distinct feature of the He II emission in Ho IX X-1 is the unresolved central component of a significant ($\simeq$370 km s^{-1}) velocity dispersion without any apparent Hβ counterpart. One possible explanation is that the central component represents a photoionized accretion disk rotating around the central X-ray source (Grise et al. 2006). The line broadening in this case is due to rotational motion, and the lack of corresponding Hβ emission suggests that it is gas of relatively small column density. The large velocity dispersion implies that the disk size is much smaller than the seeing size for any conceivable mass range for the central source, consistent with our results (Section 2).

As noted above, M81 X-6 lacks a central component altogether. In Ho II X-1 the absence of a large velocity dispersion in the central region (offset of $\leqslant 1''$) probably indicates the lack of an accretion disk, although it may be due to a projection effect, i.e., Ho II X-1 is close to a face-on system. The more likely scenario is that the extended highly ionized nebula is regularly distributed around the system's center and smoothly connects to the broad component. Another possibility of the unresolved central He II component of Ho IX X-1 is that it is due to strong He II emission from the optical (stellar) counterpart of the source. For instance, some Wolf-Rayet stars are known to produce luminous He II emission of significant velocity dispersion (e.g., Crowther & Hadfield 2006). We need more information on the optical counterpart to investigate this scenario further.

Our observations point to photoionization by intense X-ray flux being the source of the He II and Hβ emission. The alternative explanation is that both are produced by the same radiative shocks. However, in the case of M81 X-6 and Ho II X-1 the observed line intensity ratios of He II to Hβ require much greater velocities than the measured upper limits (Allen et al. 2008), making it incompatible with radiative shocks. For Ho IX X-1, the observed line intensity ratio requires comparable, but still slightly greater, velocities than observed (~230 km s^{-1} for He II) if the emission is produced in strong shocks. Therefore, our results favor the interpretation that the He II line emission is dominated by X-ray photoionization. Under this scenario, the smaller extent of the He II emission traces the locations where most of the energetic X-ray radiation from the ULXs is locally absorbed.

Under the assumption of photoionization, the observed He II luminosities can be used to obtain independent measurements of the ULX X-ray luminosities. The X-ray luminosities estimated based on the observed He II line luminosities are independent of the assumption that the X-ray radiation from the central source is isotropic—the inevitable assumption to calculate the X-ray luminosities from the observed X-ray fluxes. Measurements to date based on the line emission all indicate luminosities in excess of 10^{39} erg s^{-1}. For example, the observed He II line luminosity of $\sim 1 \times 10^{36}$ erg s^{-1} of the ULX in NGC 5408 provides a lower limit of $\sim 2.5 \times 10^{39}$ erg s^{-1} for its X-ray luminosity (Kaaret & Corbel 2009) and the He II luminosity of $\sim 2.7 \times 10^{36}$ erg s^{-1} leads to an estimated X-ray luminosity of $\sim 5 \times 10^{39}$ erg s^{-1} in Ho II X-1.

In our observations we use a relatively small (1″ in width) slit, so that the measured luminosities given in Section 2 are firm lower limits. One way to estimate the upper limits on the extended He II line luminosities is to scale up the observed luminosities within the slit under the hypothesis that the He II emission is uniformly and symmetrically distributed outside the slit. In doing so we obtain the upper limits of $\sim 1.2 \times 10^{37}$ erg s^{-1} and $\sim 4.4 \times 10^{36}$ erg s^{-1} for Ho IX X-1 and M81 X-6, respectively, within an 8″ radius. We then calculate the X-ray luminosities required to produce the He II line luminosities using the photoionization modeling program *CLOUDY* (ver. 07.02.01; Ferland et al. 1998). In the modeling, we used an input X-ray spectrum of a multicolor disk blackbody plus a cutoff power-law component for Ho IX X-1 (Dewangan et al. 2006) and disk blackbody component for M81 X-6 (Swartz et al. 2003). We also assumed a constant gas density of 10 cm^{-3}, a unity filling factor, and a spherically symmetric geometry. We find that to account for the He II line luminosities the required X-ray luminosities are in the range of $\sim 10^{39}$–10^{40} erg s^{-1}, comparable to the observed ULX X-ray luminosities. This favors models where the X-ray emission is isotropic rather than beamed, which includes the scenario where ULXs are intermediate-mass black holes.

REFERENCES

Abolmasov, P., & Moiseev, A. V. 2008, RevMexAA, 44, 301
Allen, M. G., Groves, B. A., Dopita, M. A., Sutherland, R. S., & Kewley, L. J. 2008, ApJS, 178, 20
Begelman, M. C. 2002, ApJ, 568, L97
Crowther, P. A., & Hadfield, L. J. 2006, A&A, 449, 711
Dewangan, G. C., Griffiths, R. E., & Rao, A. O. 2006, ApJ, 641, L125
Ferland, G. J., Korista, K. T., Verner, D. A., Ferguson, J. W., Kingdon, J. B., & Verner, E. M. 1998, PASP, 110, 761
Grise, F., Pakull, M. W., & Motch, C. 2006, in IAU Symp. 230, Populations of High Energy Sources in Galaxies, ed. E. J. A. Meurs & G. Fabbiano (Cambridge: Cambridge Univ. Press), 302
Kaaret, P., & Corbel, S. 2009, ApJ, 697, 950
Kaaret, P., Ward, M. J., & Zezas, C. 2004, MNRAS, 351, L83
King, A. R., Davies, M. B., Ward, M. J., Fabbiano, G., & Elvis, M. 2001, ApJ, 552, L109
Kuntz, K. D., Gruendl, R. A., Chu, Y.-H., Chen, C.-H. R., Still, M., Mukai, K., & Mushotzky, R. F. 2005, ApJ, 620, L31
La Parola, V., Peres, G., Fabbiano, G., Kim, D. W., & Bocchino, F. 2001, ApJ, 556, 47
Lehmann, I., et al. 2005, A&A, 431, 847
Liu, J.-F., Bregman, J. N., & Seitzer, P. 2002, ApJ, 580, L31
Miller, B. W. 1995, ApJ, 446, L75
Miller, N. A., Mushotzky, R. F., & Neff, S. G. 2005, ApJ, 623, L109
Moon, D.-S., & Eikenberry, S. S. 2001, ApJ, 549, L225
Moon, D.-S., Eikenberry, S. S., & Wasserman, S. M. 2003a, ApJ, 582, L91
Moon, D.-S., Eikenberry, S. S., & Wasserman, S. M. 2003b, ApJ, 586, 1280
Oke, J. B., et al. 1995, PASP, 107, 375
Pakull, M. W., & Angebault, L. P. 1986, Nature, 332, 511
Pakull, M. W., Grise, F., & Motch, C. 2006, in IAU Symp. 230, Populations of High Energy Sources in Galaxies, ed. E. J. A. Meurs & G. Fabbiano (Cambridge: Cambridge Univ. Press), 293
Pakull, M. W., & Mirioni, L. 2002, arXiv:astro-ph/0202488
Pakull, M. W., & Motch, C. 1989, Nature, 337, 337
Ramsey, C. J., Williams, R. M., Gruendl, R. A., Chen, C.-H. R., Chu, Y.-H., & Wang, Q. D. 2006, ApJ, 641, 241
Roberts, T. P., & Warwick, R. S. 2000, MNRAS, 315, 98
Sivakoff, G. R., Sarazin, C. L., & Jordán, A. 2005, ApJ, 624, L17
Swartz, D. A., Ghosh, K. K., McCollough, M. L., Pannuti, T. G., Tennant, A. F., & Wu, K. 2003, ApJS, 144, 213
Zampieri, L., & Roberts, T. P. 2009, MNRAS, 400, 677